Title
Jet impingement modeling of cryogen spray cooling: analysis of 2D cryogen temperature distribution

Authors
Choi, Bernard
Welch, Ashley J

Publication Date
2001-05-21

DOI
10.1117/12.427836

Jet Impingement Modeling of Cryogen Spray Cooling: Analysis of 2-D Cryogen Temperature Distribution

Bernard Choi* and A.J. Welch
Biomedical Engineering Laser Laboratory
The University of Texas at Austin
ENS Building, Room 610
Austin, TX 78712-1084

1. ABSTRACT

The main goal of this study was to demonstrate the feasibility of using back-side infrared imaging to estimate the spatial cryogen temperature distribution during a cryogen spurt. Calculations from numerical models showed that the front-side temperature distribution could be identified at the back side of a thin aluminum sheet. Infrared images were obtained at various timepoints during a cryogen spurt from the back side of a 800-μm aluminum sheet and the temperature distribution estimated. The temperature distribution was approximately gaussian in shape.

A secondary goal was to calculate the temperature distribution in skin for two cases: 1) uniform cryogen temperature distribution, essentially representative of a 1-D geometry assumption; and 2) nonuniform distribution. At the end of a 100-ms spurt, calculations showed that, for the two cases, large discrepancies in temperatures at the surface and at a 60-μm depth were found at radii greater than 2.5 mm. These results suggest that it is necessary to consider spatial cryogen temperature gradients during cryogen spray cooling of tissue.

Key words: focal plane array, port wine stains, blackbody calibration

2. INTRODUCTION

Cryogen spray cooling (CSC) is currently used in conjunction with pulsed laser radiation for treatment of Port Wine Stains (PWS) [1] and wrinkles [2]. Laser heating of target chromophores such as hemoglobin or water in the papillary dermis runs the risk of significant thermal injury to the overlying epidermis due to absorption of incident light by melanin and water. Rapid cooling of the epidermis with a cryogen spurt prior to laser irradiation can result in a marked reduction of the epidermal temperature rise with minimal alteration of the temperature rise in the dermis.

Most previous studies on CSC assumed a 1-D tissue geometry because the sprayed area is much larger than the expected depth over which significant cooling occurs [3-17]. A recent study by Verkruysse et al. [16] investigated the possibility of radial thermal gradients during CSC. Thermocouples were embedded at a 90-μm depth at the central axis of a cryogen spurt and at a lateral distance of 3 mm away from the central axis. The temperature-time history at these two positions differed considerably from one another, suggesting that CSC dynamics were different at these two points.

Knowledge of the surface temperature of skin during CSC is essential for proper treatment of cutaneous abnormalities. However, both contact and non-contact methods of estimating surface temperatures are limited in the amount of knowledge they provide. Thermocouples offer only a point temperature measurement, and their relatively large size (e.g. 30-90 μm bead diameters [3, 14-16]) compared to the effective depth of cooling (200-400 μm [14]) may lead to errors in temperature measurements, especially in regions of sharp temperature gradients [18]. Infrared temperature measurements are limited due to cryogen film formation on the surface; this film attenuates infrared emission from superficial layers of skin. Since the film thickness as a function of time and radius is unknown, it is not possible to obtain an accurate 2-D surface temperature map from surface infrared images.

*contact berniec@mail.utexas.edu; phone 1 512 471-9497; fax: 1 512 475 8854

An alternate technique for estimating the spatial cryogen temperature distribution is to apply a cryogen spurt to the front side of a sample and take infrared images from the back side. If the thermal conductivity of the sample is high and the initial spatial temperature gradients oriented such that axial heat conduction is the dominant heat transfer mechanism, then back-side infrared images can provide a reasonable estimate of the initial temperature distribution.

The goal of this study was to test the predictive capability of 1-D CSC models. We 1) estimated the surface temperature distribution induced by a cryogen spurt using back-side infrared imaging and 2) predicted the difference in transient internal surface temperatures between assuming a uniform (e.g. 1-D) and non-uniform cryogen temperature.

3. FEASIBILITY STUDY OF BACK-SIDE INFRARED IMAGING

To determine the feasibility of back-side infrared imaging, an explicit finite-difference model [19] was used to predict the temperature distribution within a thin aluminum sheet subjected to a cryogen spurt of varying duration. The heat conduction equation was solved using cylindrical coordinates and assuming a convective surface boundary condition. Relevant spatial and thermal parameters incorporated into the model are listed in Table 1. Thermal properties of the aluminum sheet were assumed to be comparable to that of Alloy-2024 [19].

Table 1. Parameters used in finite-difference model of CSC of aluminum sheet.

Property (units)	Value
Sample thickness [μm]	800
Sample radius [cm]	3
Pixel dimensions (radial × axial) [μm]	300 × 20
Initial temperature [°C]	22
Thermal conductivity [W/cm/K]	1.77
Density [g/cm^3]	2.77
Specific heat [J/g/K]	0.875
Thermal diffusivity [cm^2/s]	0.73
Cryogen heat transfer coefficient [W/cm^2/K]	0.24
Cryogen spurt radius [cm]	1.5
Air heat transfer coefficient [W/cm^2/K]	0.001

In the model, the cryogen spurt covered an area that was 3 cm in diameter. For regions directly under the spurt, the cryogen heat transfer coefficient h_{cry} was applied; for regions under air, the air heat transfer coefficient was used. In the literature, values of h_{cry} range between 0.24 and 9 W/cm^2/K and cryogen temperature T_{cry} between –7 and -49°C [4, 10, 14, 16]. For our initial model, we used h_{cry} = 0.24 W/cm^2/K and T_{cry} = -44°C, which were estimated from temperature measurements using thermocouples embedded in an epoxy tissue phantom [14].

Three cryogen temperature distributions were assumed: 1) uniform, 2) linear, and 3) gaussian (see Figure 1). Simulations were run using MATLAB 5.3 (The MathWorks, Inc.; Natick, MA) for five cryogen spurt durations: 20, 40, 60, 80, and 100 ms. Temperature data were saved every 10 ms of simulated time.

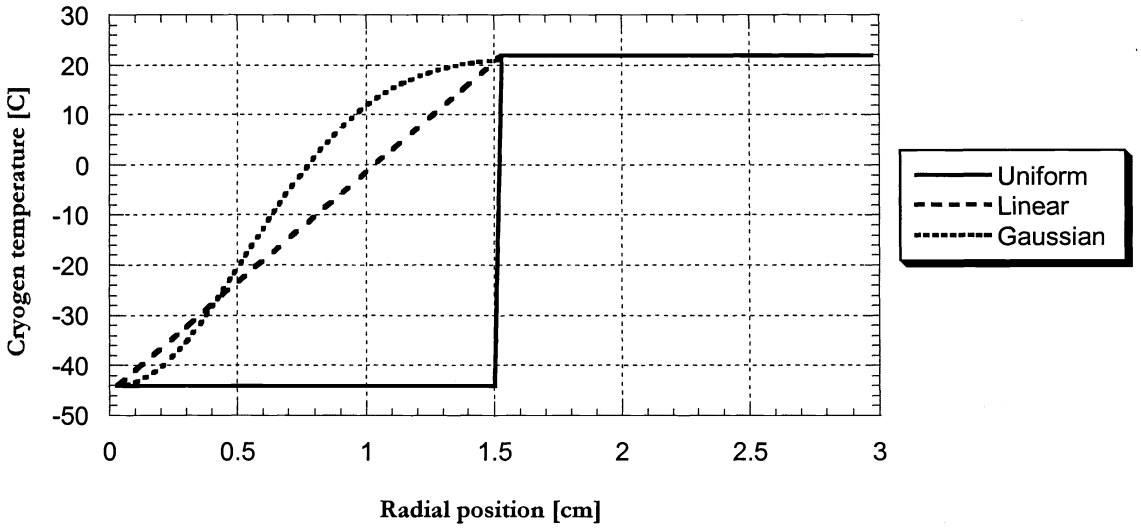

Figure 1. Cryogen temperature distributions used in finite difference model.

The calculated back-side temperature distribution at the end of a 100-ms spurt is shown in Figure 2. Each plot in Figure 2 represents a convolution of a cryogen temperature distribution (Figure 1) with a thermal blurring function due to radial heat conduction. Blurring is more pronounced with the uniform cryogen temperature distribution then for the linear or gaussian distributions due to the sharp boundary demarcating cooled versus non-cooled regions of the surface.

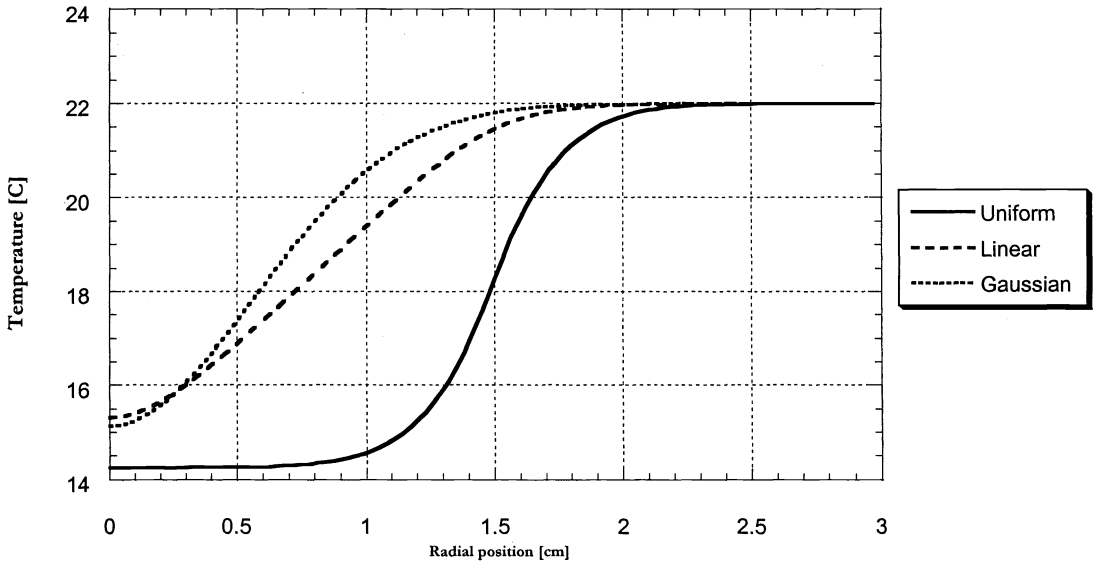

Figure 2. Calculated back-side temperature distribution of a 800-μm-thick aluminum sheet at the end of a 100-ms cryogen spurt.

A 3-D surface plot of the calculated temperature distribution inside the aluminum sheet after a 100-ms spurt is shown in Figure 3. In this case, the cryogen temperature distribution was assumed to be uniform. Note that for a given radial position, the temperature values as a function of axial position are relatively constant.

Infrared temperature measurements of an object are accurate only if no superficial temperature gradients exist [18, 20, 21]. This model run suggests that temperatures estimated from back-side infrared images may be fairly accurate representations of temperatures at the back surface.

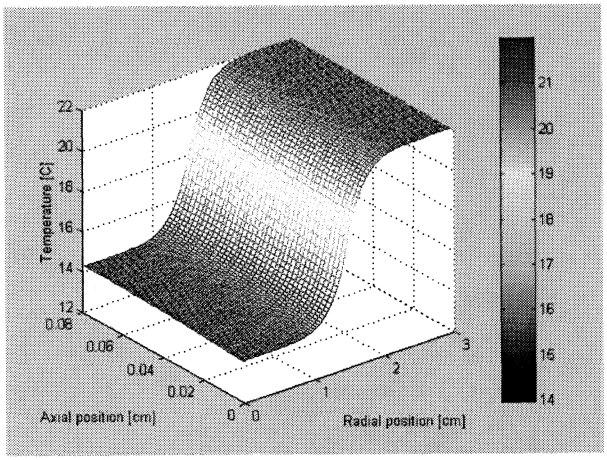

Figure 3. Surface plot of internal temperature distribution of aluminum sheet at end of 100-ms cryogen spurt. A uniform cryogen temperature distribution was assumed (see Figure 1).

Results of this feasibility study indicate that back-side infrared imaging is an adequate technique for estimating the cryogen temperature distribution during CSC. The measured temperature distribution may be a slightly-blurred representation of the actual cryogen temperature distribution. Since the difference in shape between the blurred temperature distribution (Figure 2) and initial cryogen temperature distribution (Figure 1) is small, the measured temperature distribution seves as a good first approximation.

4. INFRARED IMAGING DURING CSC OF ALUMINUM SHEET

Experimental Setup

The experimental setup is shown in Figure 4. Black spray paint (Crown 7191 Flat Black Maintenance and Touch-Up Paint, Woodstock, IL) was applied to one side of an 800-μm-thick aluminum sheet (Alloy-2204, McMaster-Carr Supply Company, Chicago, IL). The sheet was mounted vertically. The handpiece of a commerical cryogen delivery device (Dynamic Cooling Device (DCD), Candela Corp., Wayland, MA) was positioned to deliver cryogen spurts towards the front (shiny) side of the sheet. The distance between the sheet and the DCD handpiece tip was 5 cm. An InSb focal plane array (Merlin Mid-IR, Indigo Systems, Santa Barbara, CA) was positioned to acquire images from the back (black) side of the sheet. The camera optics were sensitive to 3-5 μm radiation, and the camera acquired up to 60 frames per second. The dimensions of each frame was 320 pixels by 256 pixels. The spatial resolution was approximately 40 μm per pixel. A digital delay generator (DG535, Stanford Research Systems, Sunnyvale, CA) was used to precisely trigger the onset of cryogen spurt delivery and infrared image acquisition. The relative humidity in the vicinity of the setup was approximately 30%.

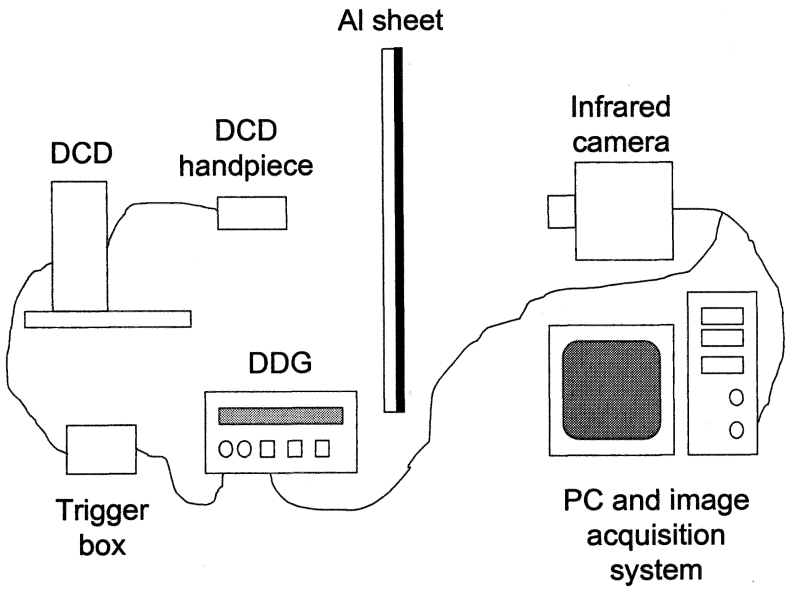

Figure 4. Schematic of experimental setup. DDG = digital delay generator, DCD = Dynamic cooling device.

Infrared image sequences were obtained for five spurt durations: 20, 40, 60, 80 and 100 ms. The images were acquired directly into PC memory and were saved to hard disk for subsequent analysis. A total of 75 image sequences were acquired and analyzed.

Blackbody calibration was performed using a thermoelectric cooler (TEC) (Model 2 SC 040 050-127-63, Melcor, Trenton, NJ). The same black paint used on the aluminum sheet was applied to the TEC surface. The surface temperature of the TEC was monitored with a thermocouple-based digital thermometer system (HH202A, Omega Engineering Inc., Stamford, CT). Blackbody images were acquired at temperatures ranging between –4.5°C and 24.2°C.

Image Processing

All image processing was done using LabVIEW 6i software (National Instruments, Austin, TX). The average gray level value of each blackbody image was calculated and a third-order polynomial equation relating gray level and blackbody temperature derived.

Gray levels of images acquired during CSC were converted to temperature values using the polynomial fit. A median filter was applied to each image to remove salt-and-pepper noise caused primarily by bad pixel elements on the focal plane array. Surface plots of average back-side temperature distributions 10, 40, and 100 ms after the onset of a 100-ms cryogen spurt are shown in Figure 5. Note that the temperature distribution is approximately gaussian in shape.

Temperature line profiles from the approximate centers of the cold regions were obtained. Average line profiles for varying spurt durations are shown in Figure 6. At 100 ms, the temperature distribution is approximately uniform over a 4-mm central region.

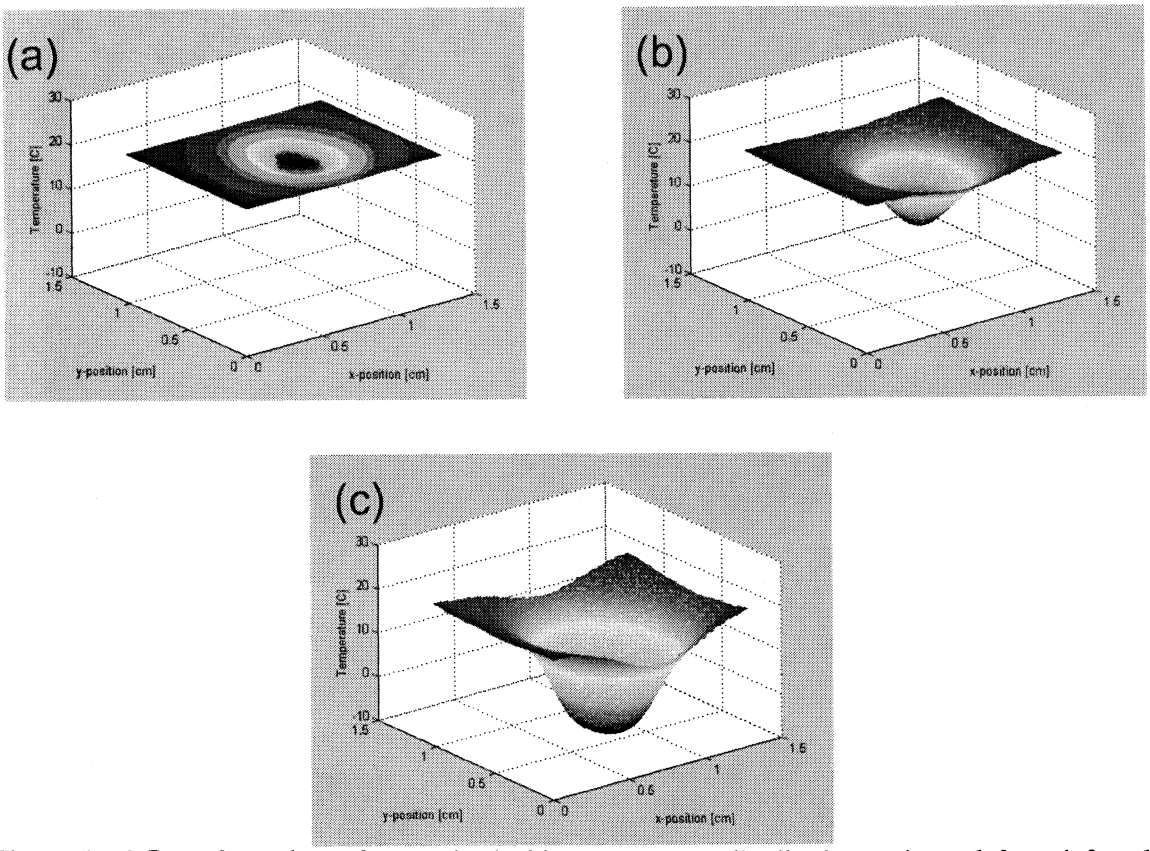

Figure 5. 3-D surface plots of mean back-side temperature distribution estimated from infrared images at a) 10 ms, b) 40 ms, and c) 100 ms after the onset of a 100-ms cryogen spurt.

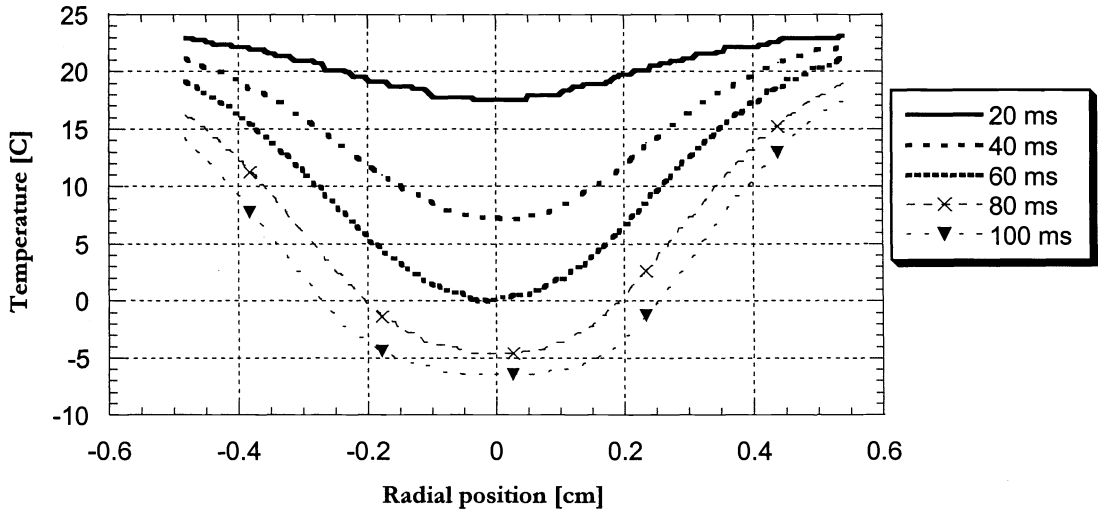

Figure 6. Average line profiles of back-side temperature distributions at the end of cryogen spurts of various durations. Line profiles were taken through the approximate center of the cooled region.

5. DISCREPANCY IN PREDICTED AND MEASURED MINIMUM TEMPERATURE VALUES

Results of the thermal model predicted a minimum temperature of 14-16°C (Figure 2). From the infrared imaging experiment, the minimum temperature was approximately -6°C, or about 20°C lower (Figure 6). One possible explanation for this difference is that the value of h_{cry} we used in the model is too low. Since the radial temperature gradient over a central 2-mm radius is approximately zero (Figure 6), we used a 1-D analytical approximation to calculate the value of h_{cry} that is necessary for the minimum temperature at the end of a 100-ms spurt to be -6°C. For convective cooling of an infinitely-wide plane wall, the temperature at depth z is [19]:

$$T(z) = T_{cry} + (T_i - T_{cry}) C_1 \exp(-\zeta_1^2 Fo) \cos\left(\frac{\zeta_1 (L - z)}{L}\right)$$

where T_i is initial temperature [C], C_1 and ζ_1 are constants, Fo is the Fourier number ($Fo = \alpha \tau_{cry}/L^2$, where α is thermal diffusivity [cm²/s] and τ_{cry} is cryogen spurt duration [s]), and L is thickness [cm]. Values of C_1 and ζ_1 were estimated using Table 5.1 in Ref. [16], from which we estimated a Biot number ($Bi = h_{cry} L/k$) of 0.047. From these calculations, we estimated h_{cry} = 1.04 W/cm²/K, which is within the range of heat transfer coefficients estimated by other researchers (0.24 - 9 W/cm²/K) [4, 10, 14, 16].

A plot of back-side temperature as a function of radial position during CSC of an aluminum sheet is shown in Figure 7. A uniform cryogen temperature distribution (Figure 1) at -44°C and heat transfer coefficient of 1.04 W/cm²/K was assumed. Note that the minimum temperature of –5.3°C in Figure 7 is comparable to the minimum value of -6°C obtained from the infrared images (Figure 6). Since this value of h_{cry} approximated the measured minimum temperature better than 0.24 W/cm²/K, we used h_{cry} = 1.04 W/cm²/K in the model described in the next section.

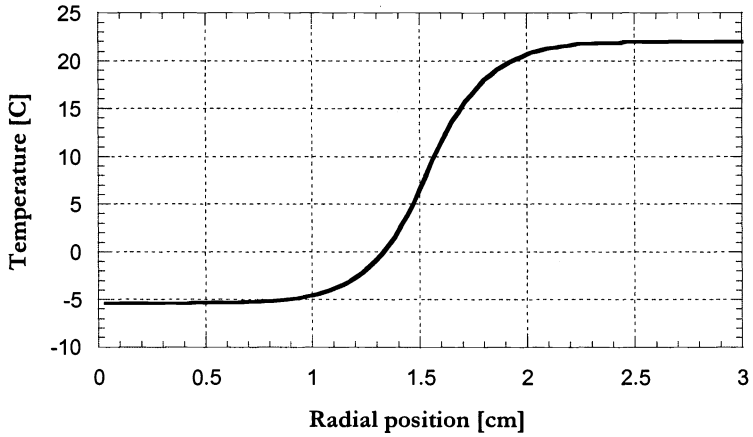

Figure 7. Predicted backside temperature distribution during CSC of an aluminum sheet. For this model run, h_{cry} = 1.04 W/cm²/K and τ_{cry} = 100 ms.

6. PREDICTION OF TEMPERATURE DISTRIBUTION WITHIN SKIN DURING CRYOGEN SPURT

Models were run to compare the predicted differences in internal temperature distribution of skin during a 100-ms cryogen spurt. The cryogen temperature distribution was assumed to be either uniform or nonuniform. For the uniform case, the cryogen temperature was set to -44°C. For the nonuniform case, the minimum cryogen temperature (e.g. at the center) was set to -44°C. The shape of the modeled cryogen temperature

distribution was assumed to match the distribution measured at the end of a 100-ms spurt (Figure 6). The temperature as a function of radius was calculated using the following equation:

$$T_{\mathrm{mod}}(r) = (T_{\infty} - T_{cry})\frac{T_{meas}(r) - T_{meas,\min}}{T_{meas,\max} - T_{meas,\min}} + T_{cry}$$

where T_{mod} is the cryogen temperature used in the model, T_{∞} is the environmental temperature, T_{cry} = -44°C, T_{meas} is the cryogen temperature measured at position r, and $T_{meas,min}$ and $T_{meas,max}$ are the minimum and maximum measured temperatures. The distribution used in the model is shown in Figure 8.

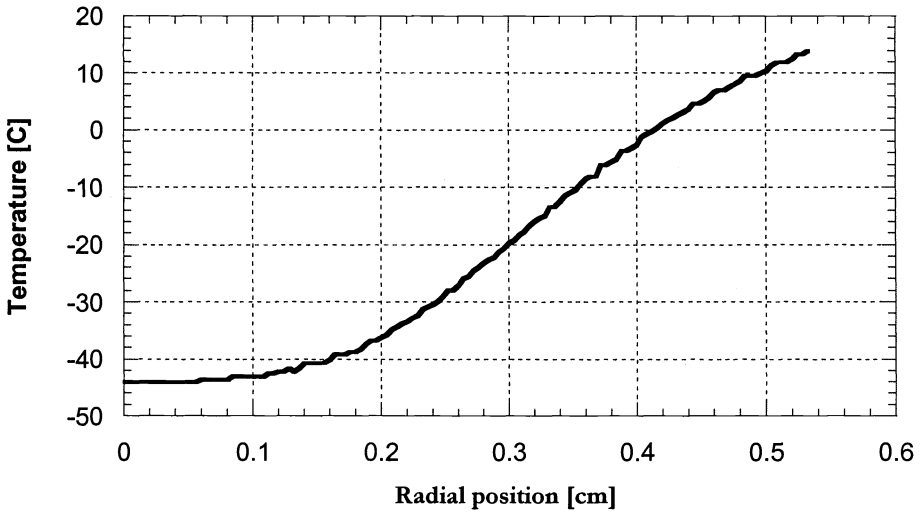

Figure 8. Nonuniform cryogen temperature distribution used in finite difference modeling of CSC of skin.

The 2-D axisymmetric finite difference model described in Section 3 was used. Relevant model parameters are listed in Table 2. The internal temperature distributions within a 5-mm radius at the end of a 100-ms spurt are shown in Figure 9 for the two cases. Figure 10 shows a difference plot ($T_{uniform} - T_{nonuniform}$) of the temperature distributions. Cooling effects are similar for both cryogen temperature distributions within a 2-mm radius. At larger radii, the difference in internal temperature distributions is as great as 40°C. Figure 11 shows radial line profiles at different depths; the depth positions were selected based on those chosen by Verkruysse et al. [17]. A depth of 60 μm corresponds to the basal layer; 150 and 400 μm are two potential PWS vessel target depths. The temperatures at the PWS vessel depths are largely unaffected by the nonuniform cryogen temperature distribution. At the basal layer, however, the uniform temperature assumption predicts basal layer temperatures that are 16 and 28°C cooler at radii of 3.5 mm and 5 mm than for the nonuniform case.

Table 2. Parameters used in finite-difference model of CSC of skin.

Property (units)	Value
Sample thickness [μm]	1000
Sample radius [cm]	2
Pixel dimensions (radial × axial) [μm]	40 × 10
Initial temperature [°C]	30
Thermal conductivity [W/cm/K]	4.60×10^{-3}
Density [g/cm^3]	1
Specific heat [J/g/K]	4.18
Thermal diffusivity [cm^2/s]	1.1×10^{-3}
Cryogen heat transfer coefficient [W/cm^2/K]	1.04
Cryogen spurt radius [cm]	0.536
Air heat transfer coefficient [W/cm^2/K]	0.001

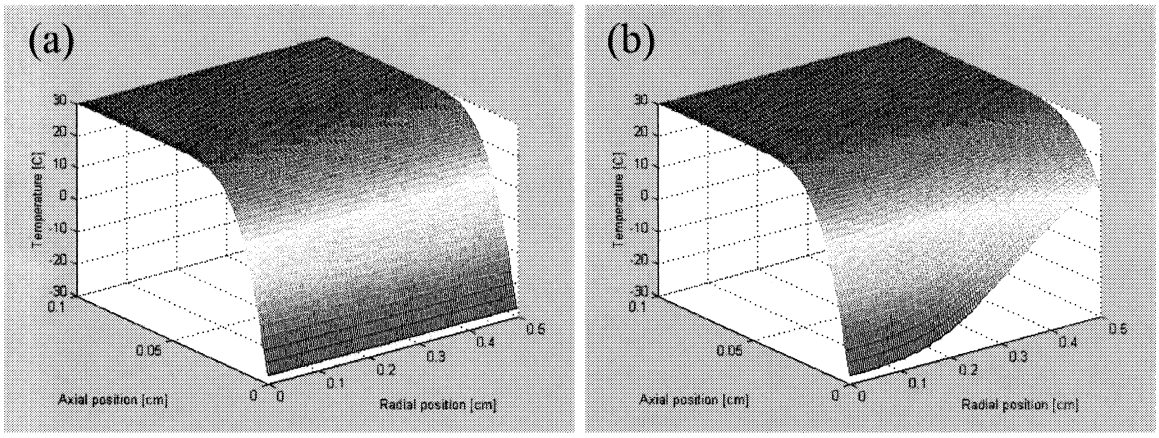

Figure 9. Skin temperature distribution at end of 100-ms cryogen spurt with the following surface boundary condition: a) uniform cryogen temperature and b) nonuniform cryogen temperature.

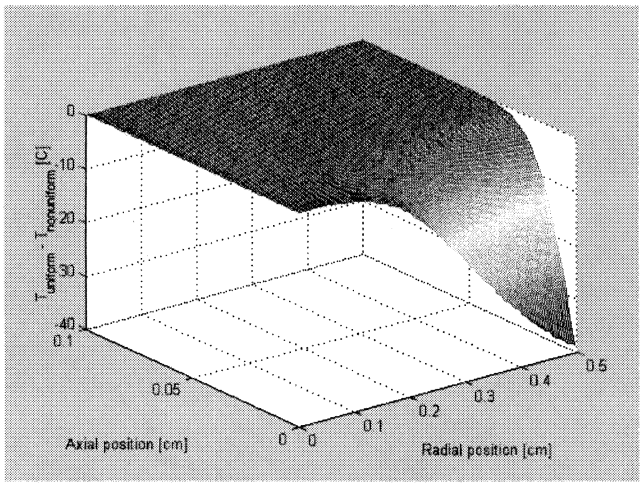

Figure 10. Temperature differential plot ($T_{uniform} - T_{nonuniform}$).

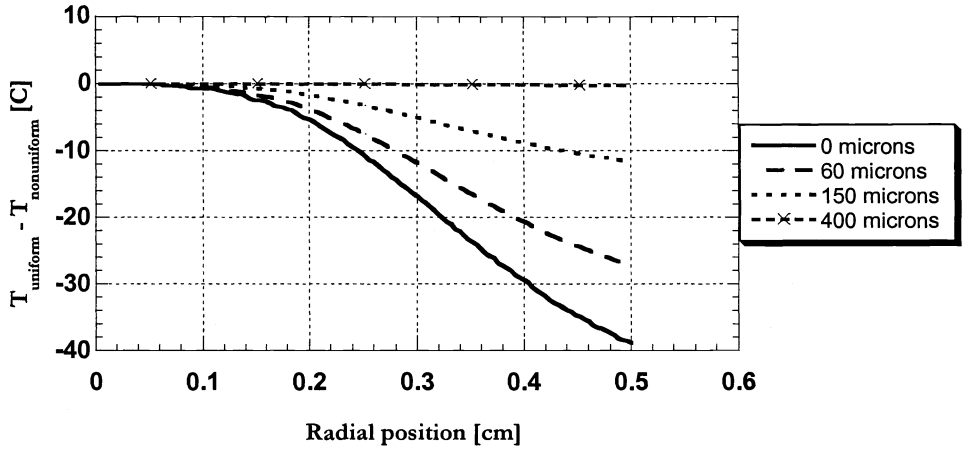

Figure 11. Radial temperature distributions at different depths within the simulated tissue.

7. DISCUSSION

Previous studies on CSC have been conducted based on the assumption that a 1-D geometry is valid. Recent work from our lab has shown that the 1-D geometry assumption for laser irradiation studies is reasonable only for relatively wide, *uniform* temperature changes [22]. If the induced temperature change contains radial gradients over a lateral distance that is not sufficiently large relative to the effective depth of temperature change, then this assumption is no longer valid.

It is very difficult to measure spatial temperature distributions during cryogen spray cooling by using surface temperature measurements. Results of preliminary models simulating CSC of an aluminum sheet demonstrated that spatial temperature gradients induced at the front surface of a thin aluminum sheet can be identified by obtaining infrared images at the back side of the sheet (Figure 2). The approximate shape of the temperature distribution is gaussian (Figures 5 and 6) during a cryogen spurt. At the end of 100 ms, the temperature is relatively constant over a 4-mm-diameter spot (Figure 6). Recent clinical PWS studies [23, 24] have involved the use of 7-mm-diameter spot size. As light propagates through a highly-scattering medium, the effective spot size is larger than the nominal value at the surface. Thus, it is important to consider spatial cryogen temperature gradients during CSC of skin.

By assuming a uniform cryogen temperature distribution, the amount of cooling at the basal layer at radial positions larger than approximately 2.5 mm is considerably overestimated (Figure 11). In order to avoid epidermal damage, this discrepancy should be taken into consideration when devising treatment plans. If the incident laser spot is gaussian-shaped, then the effect of radial cryogen temperature gradients may be mitigated due to the lower incident energy at the edges of the gaussian beam. However, for a flattop beam profile, radial gradients may play a large role in determining the overall thermal effects during treatment.

In this study, h_{cry} was assumed to be constant. In reality, the surface heat transfer coefficient may vary as a function of radial position [17, 25]. From temperature measurements during CSC of an epoxy block, Verkruysse et al. [16] calculated h_{cry} = 1 W/cm^2/K, which is approximately the value estimated in this study. They used a range of h_{cry} values centered around 1 W/cm^2/K as input into a 1-D model to determine the effect of different h_{cry} values on the predicted temperature distribution in the block. They found that the calculated temperature values varied by less than 0.5°C when h_{cry} was varied between 0.59 and 3 W/cm^2/K, indicating that relatively large changes in h_{cry} have a negligible effect on the overall temperature distribution. Thus, as a first-order approximation, it is reasonable to assume that h_{cry} is constant. Future studies need to be conducted to assess the relationship between h_{cry} and radial position.

8. CONCLUSIONS

Back-side infrared imaging can be used to estimate the cryogen temperature distribution at the front surface during a cryogen spurt. Results of this study indicate that spatial cryogen temperature gradients need to be considered during modeling of CSC. Experimental and detailed modeling studies need to be conducted to determine the ultimate effect of these gradients

9. ACKNOWLEDGMENTS

The authors would like to thank Candela Corp. for generously providing the DCD and Karl Pope and Drs. Tony Durkin and Neil Wright for their assistance. Funding for this research was provided in part by grants from the Air Force Office of Scientific Research through MURI from DDR&E (F49620-98-1-0480), the Texas Higher Education Coordinating Board (BER-ATP-253), and the Albert and Clemmie Caster Foundation.

10. REFERENCES

1. Waldorf HA, Alster TS, McMillan K, Kauvar ANB, Geronemus RG, and Nelson JS. Effect of dynamic cooling on 585-nm pulsed dye laser treatment of port-wine stain birthmarks. Dermatol Surg 1997; 23:657-662.
2. Lask G, Lee PK, Seyfzadeh M, Nelson JS, Milner TE, Anvari B, Dave D, Geronemus RG, Bernstein LJ, Mittlelman H, Ridener LA, Coulson WF, Sand B, Baumgardner J, Hennings D, Menefee R, and Berry M. Nonablative laser treatment of facial rhytides. Proceedings SPIE 1997; 2970:338-349.
3. Aguilar G, Majaron B, Verkruysse W, Zhou Y, Nelson JS, and Lavernia EJ. Theoretical and experimental analysis of droplet diameter, temperature, and evaporation rate evolution in cryogenic sprays. Int J Heat Mass Transfer 2001; in press.
4. Anvari B, Milner TE, Tanenbaum BS, Kimel S, Svaasand LO, and Nelson JS. Selective cooling of biological tissues: Application for thermally mediated therapeutic procedures. Phys Med Biol 1995; 40:241-252.
5. Anvari B, Tanenbaum BS, Milner TE, Kimel S, Svaasand LO, and Nelson JS. A theoretical study of the thermal response of skin to cryogen spray cooling and pulsed laser irradiation: Implications for treatment of port wine stain birthmarks. Phys Med Biol 1995; 40:1451-1465.
6. Anvari B, Milner TE, Tanenbaum BS, Kimel S, Svaasand LO, and Nelson JS. Dynamic epidermal cooling in conjunction with laser treatment of port wine stains: Theoretical and preliminary clinical evaluations. Lasers Med Sci 1995; 10:105-112.
7. Anvari B, Tanenbaum BS, Milner TE, tang K, Liaw LH, Kalafus K, Kimel S, and Nelson JS. Spatially selective photocoagulation of biological tissues: Feasibility study utilizing cryogen spray cooling. Appl Opt 1996; 35:3314-3320.
8. Anvari B, Tanenbaum BS, Hoffman W, Said S, Milner TE, Liaw LHL, and Nelson JS. Nd:YAG laser irradiation in conjunction with cryogen spray cooling induces deep and spatially selective photocoagulation in animal models. Phys Med Biol 1997; 42:265-282.
9. Anvari B, Ver Steeg BJ, Milner TE, Tanenbaum BS, Klein TJ, Gerstner E, Kimel S, and Nelson JS. Cryogen spray cooling of human skin: Effects of ambient humidity level, spraying distance, and cryogen boiling point. Proceedings SPIE 1997; 3192:106-110.
10. Anvari B, Milner TE, Tanenbaum BS, and Nelson JS. A comparative study of human skin thermal response to sapphire contact and cryogen spray cooling. IEEE Trans Biomed Eng 1998; 45:934-941.
11. Exley J, Dickinson MR, King TA, Charlton A, Falder S, and Kenealy J. Comparison of cooling criteria with a cryogen spray and water/air spray. Proceedings SPIE 1999; 3601:130-140.
12. Milner TE, Anvari B, Keikhanzadeh K, Dave D, Nelson JS, Goodman DM, Hennings D, Baumgardner J, and Berry M. Analysis of nonablative skin resurfacing. Proceedings SPIE 1997; 2970:367-373.
13. Nelson JS, Milner TE, Anvari B, Tananbaum BS, Svaasand LO, and Kimel S. Dynamic epidermal cooling in conjunction with laser-induced photothermolysis of port wine stain blood vessels. Lasers Surg Med 1996; 19:224-229.
14. Torres JH, Nelson JS, Tanenbaum BS, Milner TE, Goodman DM, and Anvari B. Estimation of internal skin temperatures in response to cryogen spray cooling: Implications for laser therapy of port wine stains. IEEE J Sel Topics Quant Elect 1999; 5:1058-1066.

15. Torres JH, Anvari B, Tanenbaum BS, Milner TE, Yu JC, and Nelson JS. Internal temperature measurements in response to cryogen spray cooling of a skin phantom. Proceedings SPIE 1999; 3590:11-19.
16. Verkruysse W, Majaron B, Aguilar G, Svaasand LO, and Nelson JS. Dynamics of cryogen deposition relative to heat extraction rate during cryogen spray cooling. Proceedings SPIE 2000; 3907:37-48.
17. Verkruysse W, Majaron B, Tanenbaum BS, and Nelson JS. Optimal cryogen spray cooling parameters for pulsed laser treatment of port wine stains. Lasers Surg Med 2000; 27:165-170.
18. Valvano JW and Pearce J. Temperature measurements. In: Welch AJ, van Gemert MJC, eds. "Optical-Thermal Response of Laser-Irradiated Tissue". New York: Plenum Press, 1995.
19. Incropera FP and DeWitt DP. Fundamentals of Heat and Mass Transfer. New York: John Wiley & Sons. 1996.
20. Majaron B, Verkruysse W, Tanenbaum BS, Milner TE, and Nelson JS. Pulsed photothermal profiling of hypervascular lesions: Some recent advances. Proceedings SPIE 2000; 3907:114-125.
21. Choi B, Pearce JA, and Welch AJ. Modeling infrared temperature measurements: Implications for laser irradiation and cryogen cooling studies. Phys Med Biol 2000; 45:541-557.
22. Choi B and Welch AJ. Analysis of thermal relaxation during laser irradition of tissue. Submitted to Lasers Surg Med.
23. Kauvar ANB, Lou WW, and Zelickson B. Effect of cryogen spray cooling on 595 nm, 1.5 msec pulsed dye laser treatment of port wine stains. Lasers Surg Med Suppl 2000; 12:24.
24. Kelly KM, Nanda VS, Shirin S, and Nelson JS. Vascular lesion treatment utilizing a pulsed dye laser at high fluences in combination with cryogen spray cooling. Lasers Surg Med Suppl 2000; 12:24-25.
25. Liu X, Lienhard JH V, and Lombara JS. Convective heat transfer by impingement of circular liquid jets. J Heat Transfer 1991; 113:571-582.